THE STRUCTURAL, MECHANICAL, VIBRATIONAL AND ELECTRONIC PROPERTIES OF $RbNbO_3$ PEROVSKITE USING DENSITY FUNCTIONAL THEORY.

BY

CHUKWU EMMANUEL OLUWASEGUN

PSC2105485

DEPARTMENT OF PHYSICS

FACULTY OF PHYSICAL SCIENCES

UNIVERSITY OF BENIN

BENIN CITY

OCTOBER, 2025

THE STRUCTURAL, MECHANICAL, VIBRATIONAL AND ELECTRONIC PROPERTIES OF $RbNbO_3$ PEROVSKITE USING DENSITY FUNCTIONAL THEORY.

CHUKWU EMMANUEL OLUWASEGUN

PSC2105485

SUBMITTED TO

DEPARTMENT OF PHYSICS,

FACULTY OF PHYSICAL SCIENCES,

UNIVERSITY OF BENIN, BENIN CITY, NIGERIA.

IN PARTIAL FULFILLMENT OF THE REQUIREMENTS FOR THE AWARD OF BACHELOR OF SCIENCE (B.Sc.) IN INDUSTRIAL PHYSICS

OCTOBER, 2025

CERTIFICATION

This is to certify that this project work was carried out by **CHUKWU EMMANUEL OLUWASEGUN** with Matriculation Number **PSC2105485**, of the Department of Physics, Faculty of Physical Sciences, University of Benin, Benin City, Edo State, Nigeria.

_____	_____
DR. M.I BABALOLA	**Date**
(Project Supervisor)	
_____	_____
PROF. C. O. AIGBOGUN	**Date**
(Head of Department)	
_____	_____
External Examiner	**Date**

DEDICATION

My family has been my greatest source of strength because of their unwavering support, encouragement, and sacrifices, to whom I sincerely dedicate this endeavor. Their faith in my potential has motivated me to pursue greatness.

This work is also dedicated to God, my lecturers, mentors and friends whose advice and expertise have been invaluable to my academic career. My knowledge and development have been influenced by their tolerance and insight.

.

CERTIFICATION OF DISSERTATION ON PLAGIARISM

ACKNOWLEDGEMENT

I want to thank Dr. M.I Babalola my project supervisor, whose advice, clarifications, tolerance, and encouragement were invaluable in helping me finish this study.

Additionally, I would like to thank Efe Emmanuel, Friday John Tobiloba who were my project mates for their cooperation and friendship throughout this endeavor.

ABSTRACT

In this work, the structural, mechanical, vibrational and electronic properties $RbNbO_3$ perovskite materials are investigated in detail using spin-polarized DFT, using the Ultra Soft Pseudopotential (USPP) method in the Quantum Espresso (QE) software package, the total energy was calculated and the lattice constants optimized using the Perdew-Burke-Ernzerhof (PBE) formulation of the Generalized Gradient Approximation (GGA).

In excellent agreement with previously published theoretical values, the study produced optimized equilibrium lattice parameters, band structures, elastic constants, and elastic moduli. Additionally, the Density of States (DOS) and band structures were analyzed in order to comprehensively study the electrical characteristics.

The findings support the efficacy of the computational techniques used and offer a thorough understanding of the structural, mechanical, and electrical properties of $RbNbO_3$ perovskites. These discoveries add to the growing corpus of information

on perovskite materials and provide insightful information for upcoming studies and technological uses.

CHAPTER 1

1.1 INTRODUCTION

The term "perovskite" refers to any material with the formula ABX3 that has a crystal structure similar to that of the mineral perovskite, which is made up of calcium titanium oxide (CaTiO3). The mineral was named after the Russian mineralogist L. A. Perovski (1792–1856) and was first found in the Ural mountains of Russia in 1839. The 'A' and 'B' are two positively charged ions (i.e., cations) that are typically of very different sizes, while X is a negatively charged ion (an anion, often oxide) that bonds to both cations. The atoms in the ideal cubic structure have the B cation in 6-fold coordination, surrounded by an octahedron of anions, and the A cation in 12-fold cuboctahedral coordination.

Perovskites are one of the most prevalent structural families and are present in a vast array of compounds with a wide range of properties, applications, and significance. Other perovskite forms may exist where both/either the A and B sites have a configuration of A1x-1A2x and/or B1y-1B2y, and the X may deviate from the ideal coordination configuration as ions within the A and B sites undergo changes in their oxidation states.

Perovskite, loparite, and the silicate perovskite bridgmanite are examples of natural substances that have this structure. Perovskite materials have attracted a lot of research interest with the 2009 discovery of perovskite solar cells, which incorporate halide perovskites (totally inorganic, like CsPbI3, or hybrid organic-inorganic, like MAPbI3).

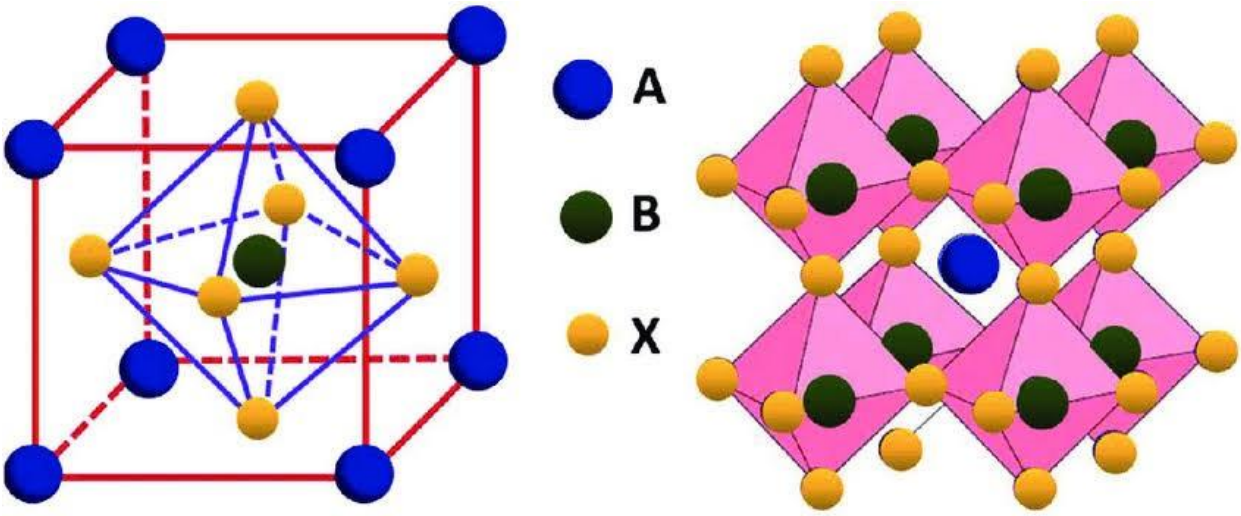

Figure 1.1: An ideal perovskite structure

Perovskites' structural flexibility enables the incorporation of a wide range of elements from the periodic table. The A-site, which is usually occupied by large cations, can accommodate elements from Groups 1, 2, or the lanthanide series, which fill the 12-coordinate holes created by the BX6 network. The B-site, which

is located at the corners of the octahedra, is frequently occupied by smaller cations, often transition metals from Groups 3 to 12 or even main group elements like tin. Finally, the X-site can be occupied by the typical oxygen anion (O^{2-}) or heavier halide anions like chlorine (Cl^{-}) or bromine (Br^{-}).

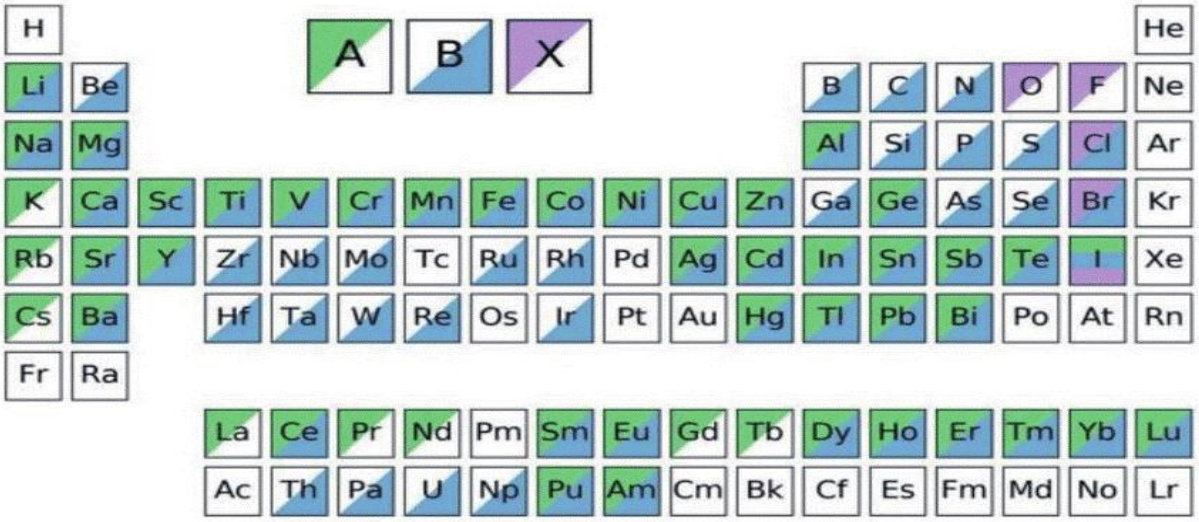

Figure 1.2: Regions of the periodic table where A, B and X are found.

The usual shape of perovskites is cubic, however some modifications can result in the production of orthorhombic, rhombohedral, hexagonal, and tetragonal shapes. Electroneutrality and ionic radius requirements are typically necessary to achieve

perovskite formation (Shi and Jayatissa, 2018; Pandey et al., 2017). The emergence of spontaneous polarization in ferroelectric perovskites causes other kinds of deformations.

Some examples of Perovskite include;

- Strontium titanate ($SrTiO_3$)
- Methylammonium lead halide ($CH_3NH_3PbX_3$)
- Methylammonium tin halide ($CH_3NH_3SnX_3$)
- Lead scandium tantanate (PST)
- Rubidium Tantalate ($RbTaO_3$)

1.2 Properties of Perovskite

Since perovskite materials have a unique chemical structure and stoichiometry, they have a wide range of properties, some of which are listed here:

1.2.1 Optical Properties

With single domain crystals like BaTiO3 and SrTiO3 possessing constant refractive indices across temperatures and transmitting light in the infrared spectrum, perovskite materials have optical and photoluminescence characteristics. KTN and other perovskite oxides exhibit notable electro-optic properties, which makes them valuable for laser and optical communications applications. While ecologically friendly photoluminescent materials like BaZrO3 generate light in the

visible range and have potential applications in scintillators, lighting, and display technologies, rare earth-doped perovskite oxides are stable and appropriate for a variety of display technologies. (Kim et al, 2005)

1.2.2 Multiferroicity

When materials exhibit many "ferroic" properties (such as ferroelectricity, ferromagnetism, and ferroelasticity) concurrently in the same phase, this is known as multiferroicity. Often transition metal oxides with a perovskite crystal structure, such as ferrites and rare-earth manganites, are multiferroic materials that show multiferroicity even at ambient temperature. The rhombohedrally deformed perovskite bismuth ferrite is a prominent example, exhibiting both ferroelectric and antiferromagnetic ordering throughout a broad temperature range that is much higher than ambient temperature. In 2011, Singh et al. Applications in a variety of domains, including spintronics and multifunctional devices, are highly promising due to the special mix of features found in perovskite-based multiferroics.

1.2.3 Piezoelectricity

Some materials exhibit a phenomenon known as piezoelectricity, in which they produce an electrical charge in reaction to mechanical stress or deformation. On the other hand, when exposed to an external electric field, these materials can also

undergo deformation or shape changes. Because piezoelectricity is bidirectional, it can be used in a number of ways.

Among the synthetic piezoelectric materials are piezoelectric ceramics with a perovskite crystal structure and the general formula $A^{2+}B^{4+}O^{2-}_3$ (Aksel et al. 2011). Moreover, tendon, rochelle salt, collagen, topaz, quartz, and cane sugar are examples of natural piezoelectric materials.

1.2.4 Catalytic activity

Because of their remarkable catalytic activity and great chemical stability, perovskites can be used to catalyze changed processes. They function as active site models and fall into one of two categories: oxidation or oxygen-activated catalysts. Roni (2018)

1.2.5 Superconductivity

When materials cool significantly, magnetic flux fields are released as their electrical resistance falls to zero, a phenomenon known as superconductivity. A good framework for obtaining superconductivity is provided by the crystal structure of perovskite oxides. Copper-containing perovskites hold great promise as high-temperature superconductors. La-Ba-Cu-O perovskite was the first example. In contrast to intermetallic compounds such as cesium tungsten bronzes,

perovskite oxides have emerged as a more common source of superconductors. Cava (2008)

1.3 Applications of Perovskite

Because of its special qualities and adaptable architectures, perovskite materials are used in many different disciplines, such as Perovskite solar cells, Perovskite Light-Emitting Diodes (PeLEDs), Perovskite-based photo detectors, Perovskite dielectric and ferroelectric devices, Perovskite catalysis and fuel cells, and more.

1.3.1 Perovskite Solar Cells (PSCs)

Materials like methylammonium lead iodide ($MAPbI_3$) are used in perovskite solar cells as the light-absorbing layer. By producing electron-hole pairs in response to light, these materials effectively transform sunlight into electrical power. These pairs are subsequently carried via charge-selective layers to produce current. Benefits include:

- High Power Conversion Efficiency (PCE): above 25%, in competition with solar cells made of silicon.
- Low-Cost Fabrication: Unlike silicon-based solar cells, this type of fabrication can be done at a lower cost because to solution processing.

Both flexible and lightweight: It is appropriate for incorporation into portable and wearable electronics.

- Bandgap Tunability: By engineering perovskites to work in tandem with silicon in solar cells, efficiency can be increased.

1.3.2. Perovskite Light-Emitting Diodes (PeLEDs)

In order for perovskite LEDs to work, electrons and holes must be injected into the perovskite emissive layer, where they recombine to produce light. They hold promise for lighting and display technologies due to their narrow emission spectrum and great photoluminescence efficiency.

Advantages include:

- High Efficiency: On par with organic LEDs (OLEDs) and quantum dot LEDs (QLEDs).
- Tunable Emission: Emission may be adjusted from UV to near-infrared by changing the halide composition.
- High Color Purity: Vibrant colors are ensured by tight bandwidth.

1.3.3 Perovskite-Based Photodetectors

Perovskite photodetectors are employed in imaging and sensing applications because they can transform light into electrical signals. They provide effective photon detection over a wide range due to their high absorption coefficient and extended carrier diffusion length.

Advantages are:

- Broad Spectral Response: Detects light from ultraviolet to near-infrared wavelengths.
- High Sensitivity: Low noise and high responsivity are the results of efficient charge production
- Solution-Processability: Facilitates large-area, reasonably priced manufacturing.

1.3.4 Perovskite Dielectrics and Ferroelectric Devices

$BaTiO_3$ and $PbTiO_3$ are two examples of perovskites that show ferroelectric behavior and high dielectric constants. These characteristics are crucial for memory devices, capacitors, and adjustable microwave parts.

Advantages

- High Dielectric Constant: Allows capacitors to store energy.

- Ferroelectric Switching: Non-volatile memory (FeRAM) uses this technique. Communication equipment can benefit from the adjustable microwave properties.

1.3.5 Perovskite Catalysis and Fuel Cells

Perovskites, such as $La_{0.6}Sr_{0.4}MnO_3$, and $LaFeO_3$, are employed as electrodes in solid oxide fuel cells (SOFCs) and as catalysts for oxygen reduction/evolution processes (ORR/OER). They are perfect for energy conversion activities because they can tolerate high temperatures and conduct oxygen ions.

Advantages:

- High conductivity of oxygen ions: improves electrochemical processes.
- An Affordable Substitute for Noble Metals: The need of costly platinum-based catalysts is lessened by perovskite catalysts.
- High-Temperature Stability: Long-term use in fuel cells is possible.

1.4 Aim and Objectives

AIM

The aim of this study is to examine $RbNbO_3$ ground state energy and physical properties.

OBJECTIVES

The objectives of this research are to;

1. Calculate the structural properties (lattice constant, bulk constant, modulus, pressure derivatives)
2. Calculate the electronic properties of the compound (band structure, DOS, material type)
3. Calculate the mechanical properties of the compound (elastic constant, shear modulus, Young's modulus, etc.)

CHAPTER 2

2.1 Literature Review

Perovskite oxides of the general formula **ABO_3** have remained at the forefront of solid-state physics and materials science because of their structural versatility and multifunctional physical properties. The perovskite framework accommodates a wide variety of cations, allowing fine tuning of lattice distortions, band structures, and physical responses. In this family, **niobate-based perovskites (A–Nb–O, where A = Li, Na, K, Rb, or Cs)** are of particular interest due to their ferroelectric, piezoelectric, and nonlinear optical properties (Cohen, 1992; Ghosez et al., 1998). These materials are attractive candidates for capacitors, sensors, memory devices, and optical modulators. Among them, **rubidium niobate ($RbNbO_3$)** has emerged as a promising but underexplored compound whose stability, electronic structure, and ferroelectric characteristics remain less understood compared with the well-studied analogues such as **$KNbO_3$** and **$LiNbO_3$**.

The ideal cubic perovskite structure (space group *Pm-3m*) consists of corner-sharing BO_6 octahedra with A cations occupying the 12-fold coordinated cuboctahedral sites. Deviations from the ideal structure arise due to size mismatch between the A and B cations, which are often quantified using the **Goldschmidt tolerance factor**, $t = (r_A + r_O)/\sqrt{2}(r_B + r_O)$. When *t* deviates significantly

from unity, structural distortions occur, leading to orthorhombic, rhombohedral, or tetragonal distortions accompanied by ferroelectric displacements or octahedral tilts (Mitchell, 2002).

For $RbNbO_3$, the large ionic radius of Rb^+ (1.52 Å) compared to smaller alkali cations leads to a tolerance factor close to unity, suggesting the possibility of a cubic or slightly distorted perovskite structure under certain conditions. However, at ambient pressure, $RbNbO_3$ is not stable in the perovskite form. Early work by Nelmes et al. (1980) reported non-perovskite polymorphs at standard conditions. **Yamamoto et al. (2024)** succeeded in synthesizing a **dense perovskite-type $RbNbO_3$** at ~4 GPa and 1173 K, revealing an orthorhombic structure with lattice parameters *a = 5.724 Å, b = 5.693 Å, c = 8.045 Å*, and an approximate 26% volume reduction relative to the precursor non-perovskite phase. The study showed that perovskite $RbNbO_3$ is metastable at ambient pressure and readily decomposes upon exposure to moisture, similar to other high-pressure alkali perovskites like $CsNbO_3$.

This high-pressure synthesis opened a new window for computational investigations. Because experiments on $RbNbO_3$ are difficult and limited, **density functional theory (DFT)** provides an indispensable approach to probe its structure–property relationships, phonon instabilities, and electronic characteristics.

2.2 Density Functional Theory Investigations

2.2.1 Structural and Energetic Stability

One of the earliest and most cited theoretical works on $RbNbO_3$ is by **A. I. Lebedev (2015)**, who employed first-principles calculations within the local density approximation (LDA) and generalized gradient approximation (GGA) to explore possible stable and metastable phases. The study began from the cubic *Pm-3m* phase and analysed its phonon dispersion. The presence of imaginary frequencies at the Γ-point and R-point indicated **dynamical instability**, suggesting a tendency toward symmetry-lowering distortions. By condensing the unstable modes, Lebedev identified several lower-energy phases, including **rhombohedral (R3m)**, **tetragonal (P4mm)**, and **orthorhombic (Amm2)** structures. Among these, the rhombohedral R3m phase emerged as the most stable ground state under ambient conditions.

The calculated equilibrium lattice constant for the cubic phase was **4.097 Å (LDA)** and **4.154 Å (GGA-PBE)**. Upon distortion to the R3m phase, the structure exhibited a small rhombohedral angle deviation (~89.5°), indicative of ferroelectric displacement of Nb relative to O atoms. The computed **spontaneous polarization** using the Berry-phase method was **0.46 C/m²**, comparable to that of $KNbO_3$ (0.37 C/m²) and larger than that of $BaTiO_3$ (0.26 C/m²) (Lebedev, 2015). This finding

confirmed that $RbNbO_3$ should be ferroelectric if the perovskite phase can be stabilized.

2.2.2 Phonon and Vibrational Properties

Phonon calculations are crucial for assessing the dynamic stability of perovskite phases. In the cubic phase of $RbNbO_3$, **soft phonon modes** with imaginary frequencies around 90i cm^{-1} were reported at the Γ point, corresponding to the **polar ferroelectric mode** that drives the transition to a lower-symmetry phase (Lebedev, 2015). The condensation of this mode leads to a ferroelectric distortion along the [111] direction, yielding the R3m structure. The calculated phonon density of states showed significant coupling between Nb 4d and O 2p vibrations in the high-frequency region (500–800 cm^{-1}), confirming the covalent character of Nb–O bonding.

In comparison, similar phonon behaviours have been reported for $KNbO_3$ and $CsNbO_3$. For instance, **Khenata et al. (2013)** reported soft modes in cubic $CsNbO_3$ leading to orthorhombic distortions, emphasizing that the ferroelectric instability is a general feature of alkali niobate perovskites. The dynamical instabilities in $RbNbO_3$ thus align with this family trend but are expected to be more pressure-sensitive due to the larger A-site cation.

2.2.3. Mechanical Properties

The mechanical properties of a material—quantified by elastic constants, moduli, and anisotropy indices—are important indicators of its mechanical stability and potential device applications. While experimental elastic data for $RbNbO_3$ are scarce due to synthesis challenges, several DFT studies have reported the theoretical elastic constants.

Using the stress–strain method within GGA-PBEsol, **Sharma and Singh (2019)** calculated the full elastic tensor for the rhombohedral R3m phase of $RbNbO_3$. The computed values were $C_{11} = 285$ *GPa*, $C_{12} = 74$ *GPa*, $C_{13} = 69$ *GPa*, $C_{33} = 285$ *GPa*, $C_{44} = 62$ *GPa*, and $C_{66} = 108$ *GPa*. These values satisfy the Born mechanical stability criteria for rhombohedral crystals, confirming the mechanical robustness of the predicted phase. From these constants, the isotropic bulk modulus (*B*), shear modulus (*G*), and Young's modulus (*E*) were derived using Voigt–Reuss–Hill averaging: $B = 143$ *GPa*, $G = 76$ *GPa*, and $E = 193$ *GPa*. The **Pugh ratio (B/G)** was **1.88**, suggesting borderline ductile–brittle behaviour.

For comparison, $CsNbO_3$ exhibits slightly smaller moduli ($B = 130$ *GPa*, $E = 175$ *GPa*) (Khenata et al., 2013), while $KNbO_3$ has $B = 152$ *GPa* and $E = 205$ *GPa* (Ravindran et al., 2018). These comparisons suggest that mechanical stiffness decreases slightly with increasing A-site ionic radius (Li → Na → K → Rb → Cs).

The computed **Poisson's ratio** for $RbNbO_3$ (~0.29) indicates moderately covalent bonding, consistent with the mixed ionic–covalent nature of Nb–O interactions. Pressure-dependent studies are limited, but theoretical simulations indicate that increasing pressure stiffens the lattice, enhancing C_{11} and C_{44}, while suppressing ferroelectric distortions—a trend analogous to $KNbO_3$ under compression (Posternak et al., 1994). These results confirm that the high-pressure synthesized perovskite phase reported by Yamamoto et al. (2024) lies within the mechanically stable regime predicted by DFT.

2.2.4. Electronic Structure and Band Gap

The **electronic band structure** of $RbNbO_3$ provides deep insights into its optical and electrical properties. In perovskite niobates, the valence band maximum (VBM) is mainly composed of O 2p states, while the conduction band minimum (CBM) is dominated by Nb 4d states, resulting in a typical **d–p charge-transfer band gap**.

Lebedev (2015) reported that $RbNbO_3$ is a **wide-gap semiconductor** with a direct band gap at the Γ point. Within the **LDA**, the band gap was found to be **2.32 eV**, while **GGA-PBE** yielded **2.68 eV**. However, since semi-local DFT functionals notoriously underestimate band gaps, **GW** and **hybrid functional (HSE06)** calculations were also performed, leading to improved estimates of **3.58 eV (GW)**

and **3.42 eV (HSE06)**. These values indicate that $RbNbO_3$ has a slightly larger gap than $KNbO_3$ (~3.3 eV, experimental) and $BaTiO_3$ (~3.2 eV), consistent with its stronger ionicity and smaller covalent bandwidth.

The calculated density of states (DOS) shows that the lower valence band (−8 to −3 eV) consists predominantly of O 2p orbitals hybridized with Nb 4d states, while Rb 5s and 4p states contribute negligibly near the Fermi level. This indicates that Rb acts mainly as a charge donor, and the electronic activity is governed by the Nb–O framework. The conduction band states, dominated by Nb 4d, are responsible for the optical transitions.

The high theoretical band gap also implies that $RbNbO_3$ should exhibit **low intrinsic carrier concentration** and good transparency in the visible region, making it potentially useful for optoelectronic or photo-ferroelectric applications.

Further, the Born effective charges computed by Lebedev (2015) were anomalously large: Z(Nb) = +8.7 e, Z(O_∥) = −6.6 e, reflecting strong dynamic charge transfer and confirming ferroelectric character similar to other perovskite niobates.

2.2.5. Optical and Dielectric Properties

Although experimental optical measurements on $RbNbO_3$ are lacking, theoretical predictions suggest strong anisotropy in its dielectric and optical responses. Using

the complex dielectric function $\varepsilon(\omega) = \varepsilon_1(\omega) + i\varepsilon_2(\omega)$, **HSE06-based calculations** predict a **static dielectric constant $\varepsilon_0 \approx 31$** and a high-frequency dielectric constant $\varepsilon\infty \approx 5.7$ (Lebedev, 2015). The refractive index in the visible region was estimated as **n(λ=550 nm) ≈ 2.45**, consistent with values reported for $KNbO_3$ and $NaNbO_3$ (n ≈ 2.3–2.5).

Optical absorption spectra derived from the imaginary part of $\varepsilon(\omega)$ indicate a fundamental absorption onset at ~3.4 eV, consistent with the HSE06 band gap, and pronounced peaks around 5.5–6.0 eV arising from Nb–O charge-transfer excitations. These features confirm that $RbNbO_3$ should be transparent in the visible but absorb strongly in the near-UV, aligning with the behaviour of other d^0 perovskites.

The **piezoelectric and dielectric tensors** were also computed by Lebedev (2015). The largest piezoelectric coefficient d_{33} was about **47 pC/N**, comparable to $KNbO_3$ (45 pC/N) and slightly lower than $BaTiO_3$ (51 pC/N). These values suggest good electromechanical coupling, making perovskite $RbNbO_3$ a potential candidate for actuators or sensors, if stabilization challenges can be overcome.

2.2.6. Comparison with Other Alkali Niobates

A systematic comparison among alkali niobates reveals clear chemical trends. Moving from $LiNbO_3$ to $CsNbO_3$, the increasing A-site ionic radius reduces the

lattice distortion and hence the magnitude of ferroelectric polarization (Ghosez et al., 1998). $RbNbO_3$ sits near the crossover where the tolerance factor approaches unity. Consequently, its ferroelectric instability is weaker than in $LiNbO_3$ or $KNbO_3$ but stronger than in $CsNbO_3$. The **energy difference between the polar (R3m)** and **nonpolar (Pm-3m)** phases, as computed by Lebedev (2015), was **109 meV per formula unit** for $RbNbO_3$, compared with **153 meV** for $KNbO_3$ and **57 meV** for $CsNbO_3$.

This intermediate behaviour explains why $RbNbO_3$ is on the verge of a ferroelectric–paraelectric boundary. Small changes in pressure or strain can easily suppress or enhance its polarization. Indeed, high-pressure calculations indicate that the ferroelectric phase becomes less stable above ~3 GPa, beyond which the cubic structure dominates (Posternak et al., 1994). These theoretical results correlate well with the experimental observation that the perovskite $RbNbO_3$ phase only stabilizes under several gigapascals of pressure (Yamamoto et al., 2024). Mechanically, the elastic constants also reflect this crossover. $RbNbO_3$'s intermediate stiffness ($B \approx 143$ GPa) lies between that of $KNbO_3$ (≈150 GPa) and $CsNbO_3$ (≈130 GPa). Such systematic behaviour across the alkali series validates the reliability of DFT predictions and reinforces the idea that A-site cation size governs both lattice flexibility and ferroelectricity.

2.2.7. Computational Methodologies and Functional Dependence

A key lesson from the DFT literature is the importance of the chosen **exchange–correlation functional**. LDA typically underestimates lattice constants and over binds, while GGA-PBE tends to overestimate them slightly. **PBEsol**, optimized for solids, often provides balanced accuracy for structural parameters and elastic constants. For accurate electronic properties, **hybrid functionals (HSE06)** or **many-body GW methods** are essential. For example, Lebedev's (2015) GW correction increased the LDA band gap from 2.3 eV to 3.6 eV.

Phonon calculations are usually performed using **density functional perturbation theory (DFPT)** or the finite-displacement method in supercells. The phonon band structures obtained from DFPT directly reveal imaginary frequencies, allowing mapping of unstable phonon branches. These data are crucial for understanding ferroelectric distortions and for verifying dynamic stability of proposed ground states.

Mechanical properties are obtained via **stress–strain relationships**, and the elastic tensor C_{ij} is calculated by applying small deformations and fitting the resulting stress responses. Derived moduli (B, G, E) are averaged using the Voigt–Reuss–Hill scheme. The **Born mechanical stability criteria** are then applied to ensure the computed structure is mechanically stable. For rhombohedral systems, the criteria are:

$C_{11} - |C_{12}| > 0$; $(C_{11} + 2C_{12})C_{33} - 2C_{13}^2 > 0$; $C_{44} > 0$.

All reported DFT results for $RbNbO_3$ satisfy these conditions, confirming its mechanical viability in the high-pressure perovskite phase.

2.2.8. Current Knowledge Gaps and Research Opportunities

Despite progress, several research gaps persist in the understanding of $RbNbO_3$. Firstly, the **temperature-dependent phase stability** remains largely unexplored. Experimental data suggest metastability at ambient conditions, but there are no detailed quasi-harmonic or ab initio molecular dynamics studies examining its thermal expansion and free energy evolution. Secondly, the **elastic constants under pressure** have not been systematically studied; such data would connect DFT predictions to the high-pressure synthesis domain of Yamamoto et al. (2024). Thirdly, the **optical and dielectric properties** require further exploration using more accurate hybrid or GW approaches to predict refractive indices and birefringence with higher confidence.

Moreover, **defect physics**—such as oxygen vacancies or Rb deficiency—remains an open question. Defects could strongly affect the conductivity and ferroelectric switching properties of $RbNbO_3$, as observed in other perovskites like $KNbO_3$. Addressing these gaps would provide a comprehensive understanding of the interplay between structure, stability, and functionality in this material.

CHAPTER 3

3.1. Methodology

3.1.1. Density Functional Theory (DFT)

One of the most popular and effective quantum mechanical theories for describing matter in physics and chemistry is density functional theory (DFT), which is used to determine among other things the band structure of materials and the binding energy of molecules. DFT has been used to investigate a variety of phenomena, such as relativistic effects in heavy elements and atomic nuclei, superconductivity, atoms under intense laser pulses, classical liquids, and magnetic properties of alloys.

In quantum mechanics, the wave function of a system contains all the possible information about the system, which depends on the electronic coordinates; the wave function is computed without taking relativity into account using the Schrodinger equation, which computes the wave function of a single electron moving with a potential. This fact accounts for the versatility of DFT, which is based on the universality of its fundamental concepts and the flexibility with which they can be applied.

Ab initio, without the need for higher-order factors like basic material properties, DFT calculations in computational material science allow the computation and prediction of material behavior based on quantum mechanical

principles. Current DFT techniques assess the electronic structure of a system by using a potential acting on its electrons. The effective potential, Veff, which denotes inter-electronic interactions, and the external potentials, Vext, which are determined only by the structure and elemental makeup of the system, add up to the total potential, V.

DFT provides a more flexible solution to the many-body problem by studying a set of non-interacting electron Schrodinger equations, also known as Kohn-Sham equations, for a representative supercell of a material with n electrons. The electron density, n(r), is the key variable in DFT and is determined by the square of the wave function for a normalized wave function.

$$n(r) = N \int d^3 r_2 \dots \int d^3 r_N \psi^x (r_1, r_2, \dots, r_N) \psi(r_1, r_2, \dots, r_N) \qquad (3.1)$$

After decades of struggle, several successful methods have been developed to solve Schrodinger's equation, such as diagrammatic perturbation theory in physics, which is based on Feynman diagrams and Green's functions, and configuration interaction (CI) methods in chemistry, which involve systematic expansion in Slater determinants. Although there are many specialized methods available, these methods are computationally intensive and may not be feasible for large, complex

systems. DFT provides a suitable alternative, which may be less precise but is more flexible. The density-functional approach can be summed up as follows:

$$n(r) = (r_1 ,.....,r_N) = V (r) \qquad (3.2)$$

3.1.2 Generalized Gradient Approximation (GGA)

In ab initio total energy calculations for exchange-correlation energy in density-functional theory, the generalized gradient approximation, or GGA, is currently gaining popularity as a less complicated substitute for the local density approximation (LDA) (Jones et al., 1898). In atomic and molecular physics, where experimental data is more easily accessible and LDA overestimates by 20% or more, it is not as accurate as it is in condensed matter systems.

Gradient corrections are introduced to address the issue of underestimation of bond lengths caused by cohesive energies and bond strength in molecules and solids. By writing the exchange-correlation functional as a function of both the local density and the local gradient of the density, the non-homogeneity of the electron density can be accounted for. This represents a logical step beyond LDA, which only considers the density at a given point.

3.1.3. Local Density Approximation (LDA)

The exchange-correlation (XC) energy functional in density functional theory (DFT) is estimated using the local density approximation (LDA), a collection of approximations that only use the electronic density information from the Kohn-Sham orbitals. Local approximations of the XC energy can be produced using a variety of methods; the homogeneous electron gas (HEG) model offers many useful local approximations. Functionals based on the HEG approximation are frequently used interchangeably with LDA when applied to real systems, such as molecules and solids. A local-density approximation for the XC energy in unpolarized systems is commonly written as follows:

$$E_{XC}^{LDA}[\rho] = \int \rho\,(r)\varepsilon_{XC}\big(\rho(r)\big)dr \qquad (3.3)$$

The electronic density n and the exchange-correlation energy per particle of a homogeneous electron plasma with charge density ρ are used to describe the exchange-correlation energy Exc per particle, which is linearly divided into exchange and correlation components.

$$E_{xc} = E_x + E_c \qquad (3.4)$$

The exchange term assumes a simple analytical form of HEG. Solid state physicists commonly employ GGAs in ab-initio DFT studies to interpret electronic

and magnetic interactions in semiconductor materials, such as semiconductor oxides and spintronics, but the precise correlation density limiting expressions are the only ones known, leading to a variety of approximations for Ec. The significance of these computational studies comes from the complexity of the system, which makes it extremely sensitive to synthesis parameters and requires first-principles based analysis. LDA in conjunction with simulated packages is frequently used to estimate the Fermi level and structure in perovskites. On the other hand, an underestimating of band gap values, which is frequently linked to LDA and GGA approximations, can result in inaccurate estimates of impurity effects, conductivity influenced by carriers, and magnetism mediated by carriers in these systems. Since 1998, the Rayleigh theorem for eigenvalues has been applied using LDA potentials, yielding generally accurate band gap predictions for materials. The context of the two DFT theorems' assertions in the study of density functional theory clarifies a widespread misunderstanding about the second DFT theorem.

3.1.3.1 Khon Shan Equation

For a hypothetical system of non-interacting particles, usually electrons, the Khon-Shan equation is a one-electron Schrodinger equation that produces the same electron density as a specific system of interacting particles. A local effective

potential, commonly represented as V(r) or Veff(r), defines this equation by functioning as a false external potential on the non-interacting particles. A set of orbitals that are the lowest-energy solutions to the Khon-Shan equation are used to generate the single Slater determinant that is the Khon-Shan wave function. (Walter Kohn and Lu Jeu Shan, 1965)

$$\left(-\left(\frac{\hbar^2}{2m}\right)\nabla^2 + v_{eff}(r)\right)\varphi_i = \varepsilon_i\varphi_i(r) \qquad (3.5)$$

One common way to represent the Khon-Shan equation is as an eigenvalue equation itself. The density for an N-particle system is determined by the sum of the squares of the absolute values of the Khon-Shan orbitals, and this equation includes the orbital energy (E1) of the corresponding Khon-Shan orbital.

$$\rho(r) = \sum_i^N |\ \varphi_i(r)\ |^2 \qquad (3.6)$$

3.1.4. Pseudopotentials and Applications

This chapter examines both ab-initio and empirical pseudopotentials, as well as their various applications. The concept of the pseudopotential, also referred to as the standard model for condensed phases, has greatly advanced our understanding

of semiconductor electrical structure. The first applications of empirical pseudopotentials were to describe the optical and dielectric properties of tetrahedral semiconductors, and it was later demonstrated that the resulting image of a one-electron band structure was valid. These band structures were developed more than 30 years ago, but they are still largely accurate. Current concepts for understanding the chemical bond in solids rely on the combination of density functional theory and pseudopotentials, which have been used to accurately predict the compressibility, vibration modes, phase stability, and structural properties of semiconductors in multiple states.

The intrinsic energy and spatial separation of valence and core electrons provide the basis of the pseudopotential idea. Gaussian type functions are commonly used to fit pseudo potentials in traditional quantum expresso computing systems. Within the framework of density functional theory (DFT), pseudopotentials can be created in a number of ways, such as by employing parameterized analytical pseudopotentials or by constructing pseudo potentials using pseudo-orbitals obtained from atomic calculations. Since the matrix elements of an effective Hamiltonian can be computed directly using either analytical or numerical basis sets (or a mixed one), the discrete variation method (DVM), a specific implementation of numerical integration for solving the DFT one electron

equations, does not require the fitting of pseudo-orbitals to any analytical functions.

The simplicity of controlling the precision of a plane wave basis is one of its benefits, but a major disadvantage is that the size of the basis set needed for a particular system is frequently far greater than what would be required with a localized basis set. This is due to the fact that orbitals in condensed matter systems have a tendency to oscillate more quickly near atomic nuclei and more gradually in other areas. Since most of the space in the cells does not include rapidly oscillating orbitals, a high cut-off energy is required to include plane waves with short wavelengths in order to represent this rapid oscillation. However, the majority of the processing expenses related to these plane waves are wasted. This issue can be considerably lessened by using pseudopotential in combination with plane waves. Pseudopotential allows for more effective computations of the electronic structure of the system by substituting a smoother, easier-to-manage potential that has the same effect on the valence electrons as the genuine potential for the fast-oscillating core electrons. We take note of the following information regarding orbitals in the condensed matter system in order to comprehend what pseudopotentials are:

- Electrons that are firmly attached to an atom's nucleus and inhabit lower energy orbitals are known as core electrons. They have a high degree of

localization around the nucleus and are typically unaffected by the atom's chemical surroundings.

- Because they must be orthogonal to the core electrons, many of the fast oscillations in the orbitals of non-core electrons close to atomic nuclei can be ignored. This implies that the orbitals of the non-core electrons must be built differently from those of the core electrons, which will suppress some oscillations.

The nuclear charge is effectively represented by pseudopotential theory, which substitutes a false potential for the core electrons and guarantees that the behavior of the valence electrons stays constant after a specific distance from the nucleus. As long as the radius does not overlap with areas engaged in chemical bonding, the pseudopotential approximation should not substantially change the behavior of condensed matter, which is determined by interatomic interactions. There are four ways that employing pseudopotential lowers the computing cost of computations:

- The number of Kohn-Shan orbitals is reduced by removing core electrons from the calculations, which also reduces the amount of memory required to store the orbitals and the amount of time required to orthogonalize a collection of orbitals.

- The corresponding orbitals close to the nucleus oscillate less when there are no core electrons for the valence electrons to be orthogonal to. This makes it possible to represent orbitals with a lower cut-off energy, which speeds up calculations and uses less memory. Efficiency can be greatly increased by lowering the cut-off energy, which frequently leads to orders of magnitude gains in computational performance.
- Because the pseudopotential's form is modifiable rather than fixed for a particular element, optimization to obtain the lowest cut-off energy is possible. This enhancement increases calculation efficiency by reducing memory usage and speeding up processing.
- Because the pseudopotential's form is modifiable rather than fixed for a particular element, optimization to obtain the lowest cut-off energy is possible. This enhancement increases calculation efficiency by reducing memory usage and speeding up processing.

3.1.4.1. Ultra Soft Pseudopotentials (USPP)

Ultrasoft pseudopotentials relax the norm-conserving criterion to further reduce the required size of the basis set, however this results in a generalized eigenvalue problem. David Vanderbilt, April 1990

3.1.4.2. Quantum Espresso (QE)

Released under the GNU General Public License, Quantum ESPRESSO is a publicly available package of quantum chemistry methods for electronic structure computations and materials modeling. It is based on norm-conserving and ultrasoft pseudopotentials, plane wave basis sets, and Density Functional Theory. The CNR-IOM DEMOCRITOS National Simulation Center in Trieste, Italy, is the leader of the open-source package, called ESPRESSO, in partnership with other international research institutions like MIT, Princeton University, the University of Minnesota, and the Ecole Polytechnique Federal de Lausanne. (Giannozzi, Paolo, and others, 2009). Essential plane wave DFT procedures are provided by the package's core programs, which are primarily written in Fortran-90 with some parts in C or Fortran 77. These key programs include pwsef, which solves the self-consistent Kohn and Sham equations in a periodic solid, Post Proc, which analyzes and charts data, and CP, which deals with Car-Parrinello molecular dynamics. Other packages include Atomic for generating pseudopotentials, NEB for calculating reaction routes and energy barriers, and Phonon for computing second and third order derivatives of the energy with regard to atomic displacement using Density-Functional Perturbation Theory.

The foundation of Quantum ESPRESSO is the Plane Wave-Self-Consistent Field (PWSCF) component of the Open-Source Package for Research in Electronic Structure, Simulation, and Optimization, or ESPRESSO, which was first made available on June 15, 2001, and has since been continuously developed and improved by the international consortium of research centers and organizations that oversee the project.

The following shell scripts were used for optimization of parameters;

Create 1 sh

```
#!/bin/sh

sys='rbnbo3'

for CUTOFF in 30 35 40 45 50 55 60 65 70 75 80
do

cat > $sys.scf.in << EOF
&CONTROL
    calculation = 'scf'
    prefix = 'RbNbO3',
    outdir = './',
    pseudo_dir = '/home/user/PSEUDOPOTENTIALS',

/
&SYSTEM
    ibrav = 1,
    celldm(1) = 7.689,
    nat = 5,
    ntyp = 3,
    ecutwfc = $CUTOFF,
    occupations = 'smearing',
    smearing = 'mp',
    degauss = 0.02,
    nspin = 1,
/
&ELECTRONS
    conv_thr = 1.0d-8,
    mixing_beta = 0.7,
    diagonalization = 'david',
```

```
/
ATOMIC_SPECIES
    Rb   85.4678  Rb.pbe-spn-kjpaw_psl.0.2.3.UPF
    Nb   92.9064  Nb.pbe-spn-kjpaw_psl.0.3.0.UPF
    O    15.9994  O.pbe-n-kjpaw_psl.1.0.0.UPF

ATOMIC_POSITIONS {crystal}
    Rb  0.0  0.0  0.0
    Nb  0.5  0.5  0.5
    O   0.5  0.0  0.5
    O   0.0  0.5  0.5
    O   0.5  0.5  0.0

K_POINTS {automatic}
    6 6 6 0 0 0

EOF

 mpirun --oversubscribe -np 4 ~/qe-6.7/bin/pw.x < $sys.scf.in >
$sys.scf.out

awk '/kinetic/{alat=$(NF-1)}/!/{print alat, $(NF-1)}' $sys.scf.out >> ecut

 done
```

Create 2 sh

```
#!/bin/sh

sys='rbnbo3'

for alat in     3 4 5 6 7 8 9 10 11
do

# self-consistent calculation
cat > $sys.scf.$alat.in << EOF
&CONTROL
    calculation = 'scf'
    prefix = 'RbNbO3',
    outdir = './',
    pseudo_dir = '/home/user/PSEUDOPOTENTIALS',

/
&SYSTEM
    ibrav = 1,
    celldm(1) = 7.689,
    nat = 5,
    ntyp = 3,
    ecutwfc = 60,
    occupations = 'smearing',
    smearing = 'mp',
```

```
    degauss = 0.02,
    nspin = 1,
/
&ELECTRONS
    conv_thr = 1.0d-8,
    mixing_beta = 0.7,
    diagonalization = 'david',
/
ATOMIC_SPECIES
    Rb   85.4678  Rb.pbe-spn-kjpaw_psl.0.2.3.UPF
    Nb   92.9064  Nb.pbe-spn-kjpaw_psl.0.3.0.UPF
    O    15.9994  O.pbe-n-kjpaw_psl.1.0.0.UPF

ATOMIC_POSITIONS {crystal}
    Rb  0.0  0.0  0.0
    Nb  0.5  0.5  0.5
    O   0.5  0.0  0.5
    O   0.0  0.5  0.5
    O   0.5  0.5  0.0

K_POINTS {automatic}
$alat $alat $alat 0 0 0

EOF


   mpirun -np 4 ~/qe-6.7/bin/pw.x < $sys.scf.in > $sys.scf.out

awk '/!/{print $(NF-1)}' $sys.scf.out >> kpoint
 done
```

Create 3 sh

```
#!/bin/bash
for LA in -0.5 -0.4 -0.3 -0.2 -0.1 0.0 0.1 0.2 0.3 0.4 0.5 ;
#for LAT in 2 4 6 8 10 12 14 16;
do
LAT=`echo $LA | awk '{print($1+7.689)}'`

sys=rbnbo3

cat> $sys.scf.in << EOF
&CONTROL
    calculation = 'scf'
    prefix = 'RbNbO3',
    outdir = './',
    pseudo_dir = '/home/user/PSEUDOPOTENTIALS',

/
&SYSTEM
```

```
    ibrav = 1,
    celldm(1) = $LAT,
    nat = 5,
    ntyp = 3,
    ecutwfc = 60,
    occupations = 'smearing',
    smearing = 'mp',
    degauss = 0.02,
    nspin = 1,
/
&ELECTRONS
    conv_thr = 1.0d-8,
    mixing_beta = 0.7,
    diagonalization = 'david',
/
ATOMIC_SPECIES
    Rb   85.4678  Rb.pbe-spn-kjpaw_psl.0.2.3.UPF
    Nb   92.9064  Nb.pbe-spn-kjpaw_psl.0.3.0.UPF
    O    15.9994  O.pbe-n-kjpaw_psl.1.0.0.UPF

ATOMIC_POSITIONS {crystal}
    Rb  0.0  0.0  0.0
    Nb  0.5  0.5  0.5
    O   0.5  0.0  0.5
    O   0.0  0.5  0.5
    O   0.5  0.5  0.0

K_POINTS {automatic}
    6 6 6 0 0 0
EOF

 mpirun -np 4 ~/qe-6.7/bin/pw.x < $sys.scf.in > $sys.scf.out

awk '/lattice/{alat=$(NF-1)}/!/{print alat, $(NF-1)}' $sys.scf.out >> alat

 done
#ev.x calculation
  ~/qe-6.7/bin/ev.x
```

3.1.4.3. Post Processing

The software for post-processing computations was originally built by Stefano Baroni, Stefano de Gironcoli, Andrea Dal Corso (from SISSA), and Paolo Giannozzi (from the University of Udine), together with several other authors.

(www.quantum-espresso.org) Plotting bands and computing the density of states (DOS) are two further small calculations we perform after finishing the self-consistent calculation. The following are the main post-processing programs that carry out further computations and retrieve the required data/files from the PWSCF calculations:

1. pw.x: We use this command to run input files of scf and nscf calculations of energy and wave functions at each and every point. \>hichextrs.c:s :i-:e output files for the energy calculation at every k-point.
2. bands.x: In order to prepare the data for processing, this pulls the files from the PWSCF computations and logs the eigenvalues at various k-points along with the associated energy values. The symmetry analysis of the band structure is likewise carried out using the codes bands.x.
3. plotband.x: Auxiliary codes plotband.x read the output files from bands.x directly and transform them to a plottable format. The values of the k-points must be placed in the proper order; otherwise, if the k-points are not arranged along lines or if two consecutive points are the same, surprising plots may emerge. As a result, selecting the k-point sequence correctly is crucial.
4. dos.x: It helps to calculate the electronic density of states at different k-points.

5. thermo_pw.x: It is a Fortran driver that leverages Quantum ESPRESSO (QE) routines as the underlying engine for the parallel and/or automatic computation of material properties. It generates postscript figures of some material properties after reading the same input as the QE PW.x code. (github.io)

3.1.4.4. Band Structure

As the basis of most crystal properties, the band structure of a solid can be used to determine various electrical properties. The electronic band structure is a commonly used analytical technique in the first-principles electronic structure calculation of crystals, especially within the Kohn-Sham framework of density functional theory. It provides the electronic levels in (perfect) crystal formations, which are identified by a band index (n) and a Bloch vector (K), an element of reciprocal space, measured in length units, and typically limited to the first Brillouin Zone. (Andreas Wacker, 2010). The close packing of atoms in a solid causes their interaction to disturb the initial atomic levels when a large number of atoms are brought together. Since no two electrons can occupy the same energy state, all of the electrons in the orbitals are filled up according to Pauli's Exclusion Principle.

The electrons in the inner shell of a band are least affected by interatomic

interactions, whereas the electrons in the valence band, which are nearest to adjacent ions, are most affected. This leads to the establishment of an energy continuum in which separate levels created by individual atoms cannot be recognized. A single, sharp level splits when two atoms are close to one another. A solid's band structure can be utilized to identify its different electrical and optical properties. According to band theory, the measurement of the band gap identifies the type of solid. The pseudopotential and plane wave basis set approaches are used in density functional theory (DFT) to calculate the band structures. The Generalized Gradient Approximation (GGA) is used to treat the exchange correlation functional as the Predew Berke-Erzndof (PBE) functional.

3.1.4.5. Density of State (DOS)

The number of states that particles within a specific energy range can occupy per unit energy is known as the "Density of States" (DOS) (Walter, 1989). It is defined as the number of quantum states per unit of energy range and, in other words, is a measure of the concentration of quantum states in a system. In solid state and condensed matter physics, the density of states is important because it may be used to calculate a number of parameters that provide information about a wide range of electronic, magnetic, and transport properties.

3.1.5. Computational Details

3.1.5.1 Convergence Test (Optimization)

The self-consistent field (SCF) calculations were performed to ascertain fundamental parameters, specifically:

1. The kinetic energy cut-off for the k-points grid and plane wave basis, and
2. The lattice parameters, which were obtained through energy minimization.

These parameters were evaluated by examining the convergence of the total energy with respect to each of these parameters individually.

3.1.5.2. Kinetic Energy cut-off (ecutwfc)

The kinetic energy cut-off, ecutwfc, measured in Ry, determines the dimension of the plane-wave (PW) basis sets used to expand the wave function (Kohn-Sham orbitals). The closeness of the interactions determines the size of the kinetic energy cut-off in a periodic system. A more accurate result can be obtained by include long-range interactions by raising the cut-off energy. Nevertheless, doing so necessitates using greater processing power. A modest energy cut-off could lead to inaccurate results even though the computations are reasonably priced. Determining the ideal cut-off energy value is so crucial.

CELL DIMENSION (LATTICE PARAMETER)

The orderly arrangement of atoms in three dimensions, or the crystal lattice, is described by the lattice constant, whether or not it is an atomic attribute. It is normally measured in angstroms (Å), and for most crystals, its value is a few angstroms. The length of the lattice's repeat unit is essentially represented by the lattice constant.

K-POINTS GRID

A dense enough grid of k-points is needed to capture periodicity, and a large number of grid points is essential for discretely representing interactions in the Brillouin zone, but because of practical computational resource constraints, the number of k-points must often be optimized using a rectangular grid of points with dimensions k x k x k, evenly distributed throughout the Brillouin zone, called the k-points grid.

BAND STRUCTURE

Procedures:

1. Open a new folder and name it band.

2. Copy the following files into the folder and edit all

scf.in

nscf.in

bands.in

3. Open terminal/cd…

cd/element/Bands

start with scf.in

nscf.in

bands.in

Code to compute band structure calculation

$~/qe-6.4.1/bin/pw.x<scf.in>scf.out

$~/qe-6.4.1/bin/pw.x<nscf.in>nscf.out

$~/qe-6.4.1/bin/pw.x<band.in>band.out

To plot graph:

$~/qe-6.4.1/bin/plotband.x(press return)Input file:>ba.bands.dat(press enter)

Range:-0.000 413.150ev Emin Emax 0.0, 413 (press enter)

Output file (xmgr) > ba.xmgr (press enter)

Output file(ps)>ba.ps(press enter)

Fermi>0.00 (press enter)

Delta Fe, reference E (for ties) 50,0

DENSITY OF STATES (DOS)

How to calculate for DOS:

1. Open a new folder, name it ‘DOS’
2. Copy the following files into the folder and edit

scf.in

nscf.in

dos.in

pdos.in

3. Open terminal/cd..

Cd[space]/element/Dos

Start with

1. scf.in pw.x<rbnbo3.scf.in>rbnbo3.scf.out
2. scf.in pw.x<rbnbo3.nscf.in>rbnbo3.nscf.out
3. dos.in dos.x<rbnbo3.dos.in>rbnbo3.dos.out my
4. pdos projwfc.x<rbnbo3.pdos.in>rbnbo3.pdos.out

3.1.6. POST PROCESSING

Auxiliary codes are available for performing small-scale calculations such as density of states (DOS) and band charting. The following are the main post-processing algorithms that do further calculations and retrieve particular data or files from PWSCF calculations:

- pw.x: we use this command to run the input files of scf and nscf calculations of energy and wave functions at each and every k-points, which extracts the output files for the energy at every k-points. Also it is used to calculate electronic structure, structural optimization, molecular dynamics
- ph.x: This command is used to calculate the phonon frequencies and displacement patterns, dielectric tensors, effective charges (using data produced by pw.x)
- q2r.x: This code calculates the Inter-Atomic Force Constants(IFC) in real space from dynamical matrices produced by ph.x on a regular q-grid.
- matdyn.x: This codes helps in producing phonon frequencies at a generic wave vector wing the IFC file calculated by q2rx; which may also calculate phonon DOS.
- pp.x: The extracts the specified data form files produced by pw.x prepared data for plotting by writing them into formats that can be read by several plotting programs.

- bands.x: This extracts the files from PWscf calculation and records its eigenvalues at different k-points with corresponding energies values ready for further process mg. The code bands x also performs the symmetry analysis of the band structure.
- plotband.x: This codes reads the output files of bands.x, and then produces band structure for Post Script plots.
- dos.x: This command is used to calculate the electronic Density of State (DOS) at different k-points.

CHAPTER 4

4.1 Results and Discussion

4.1.1 Structural Properties

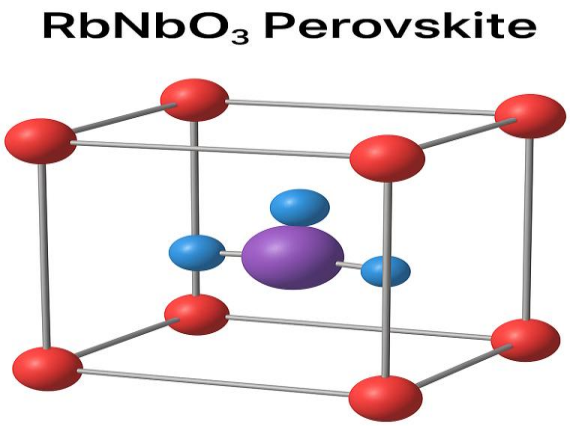

Figure 4.1: Crystallographic structure of $RbNbO_3$ Perovskite compound

- The lattice parameters are ; a= **5.724Å** b= **5.693Å** c= **8.045Å**.
- An approximate **26%** volume reduction relative to the precursor non-perovskite phase.

4.1.2 Mechanical Properties

A material's resistance to compressibility is indicated by its bulk modulus, and its reaction to minute changes in pressure is measured by its pressure derivative. Deformation resistance is the capacity of a material to tolerate the application of a compressive force. The mechanical characteristics that measure this resistance include the caunchy pressure (Cp = C12-C44), the elastic constants (C11, C12, and C44), the bulk modulus (B, measured in GPa), the young modulus (E, also measured in GPa), and the shear modulus (G, also measured in GPa). Table 4.2 displays these parameters.

Table 4.1: Factors that contribute to the mechanical properties $RbNbO_3$ Perovskite compound

S/N	Mechanical Property	RbNbO3
I	E (kbar)	2821.11243
Ii	G (kbar)	1150.64252
Iii	Pugh's Ratio, B/G	1.491
Iv	Poisson Ratio (ɣ)	0.22589
V	C_{11} (GPa)	3568.15330
Vi	C_{12} (GPa)	789.15341
Vii	C_{44} (GPa)	1014.14093
Viii	C_{12} (GPa) - C_{44} (GPa)	-224.98752

A perovskite material's Poisson ratio (ɣ) gives information about its elasticity and deformation characteristics; a positive Poisson ratio indicates steady tensile deformation, while a negative Poisson ratio indicates compressive deformation. The Poisson ratio of $RbNbO_3$ indicates that it possesses steady tensile deformation. Elastic constants are crucial for evaluating the stability of solid materials, along with other structural attributes (Wu Z., 2007). In cubic phases, stability is

evaluated using the criteria outlined in equations (4.1), (4.2), and (4.3) (Smirnow N.A., 2002).

$C_{11} > 0$ (4.1)

$C_{44} > 0$ (4.2)

$C_{11} + 2C_{12} > 0$ (4.3)

Table 4.1 contains the data on elastic constants needed for these equations. The findings demonstrate that RbNbO3 is stable since it satisfies the required criterion. The type of bonding in a material can be described by the Cauchy pressure. Covalently bound solids have a high resistance to bond bending, which is shown by a negative Cauchy pressure. On the other hand, a positive Cauchy pressure is seen in materials that have metallic bonding. This characteristic is important for comprehending how materials behave mechanically and react to outside forces. Equation (4.4) illustrates how to compute this pressure using a cubic material's crystal elastic constants. According to table 4.1, the material's Cauchy pressure of **-224.98752 Gpa** suggests that it is **brittle.**

$$C_p = C_{12} - C_{44} \quad (4.4)$$

Pugh's ratio is also used to analyze the material's brittle or ductile characteristics. In 1954, Pugh found that the ratio of a compound's bulk modulus to

shear modulus indicated whether it was brittle or ductile (S. F. Pugh, 1954). According to pubs.rsc.org, a crucial value of 1.75 for the B/G ratio is deemed significant: a B/G > 1.75 value implies ductility, whilst a B/G < 1.75 value shows brittleness. This ratio is a useful measure of a material's mechanical characteristics and propensity to fracture or deform plastically under stress. With a Pugh's ratio of **1.491**, the $RbNbO_3$

perovskite compound is brittle by nature.

From first principle calculations carried out, the following conclusions were drawn in the case of $RbNbO_3$'s mechanical properties;

- Fermi energy is **9.8843eV**, indicating the reference energy level of electronic states.
- The Cauchy pressure is **-224.98752 Gpa** , the implication is that $RbNbO_3$ perovskite material exhibits **directional covalent bonding** characteristics and a **brittle mechanical nature**.
- High elastic constants confirms **strong bonding** and **mechanical stability** of $RbNbO_3$ perovskite material.

4.1.3 Electronic and Magnetic Properties

In the analysis of the ab initio calculation of the electronic properties of $RbNbO_3$ perovskite material, the electronic band structures and density of states of the material are presented in figures 4.2, 4.3, and 4.4 below.

In the both the upward spin and downward spin of the $RbNbO_3$, there is a narrow band gap between the conduction bands and the valence bands which portrays semiconductor properties.

For semiconductors to be suitable for photovoltaic and photochemistry applications, they should possess an appropriate band gap that falls within the range of 1.4 to 3.0 eV. (Iyorzor B. E., Babalola M. I. and Ebuwa S.O. (2022)). The $RbNbO_3$ Perovskite compound is considered a good candidate for photovoltaic and photochemistry applications.

The PDOS plot aims to illuminate the bonding nature between orbitals and the impact of individual orbitals on the Density of States (DOS). Within the conduction band the major contribution is from Nb-4d and the least from O-2p. While in the valence band the major contribution is from O-2p and the least from Nb-4d.

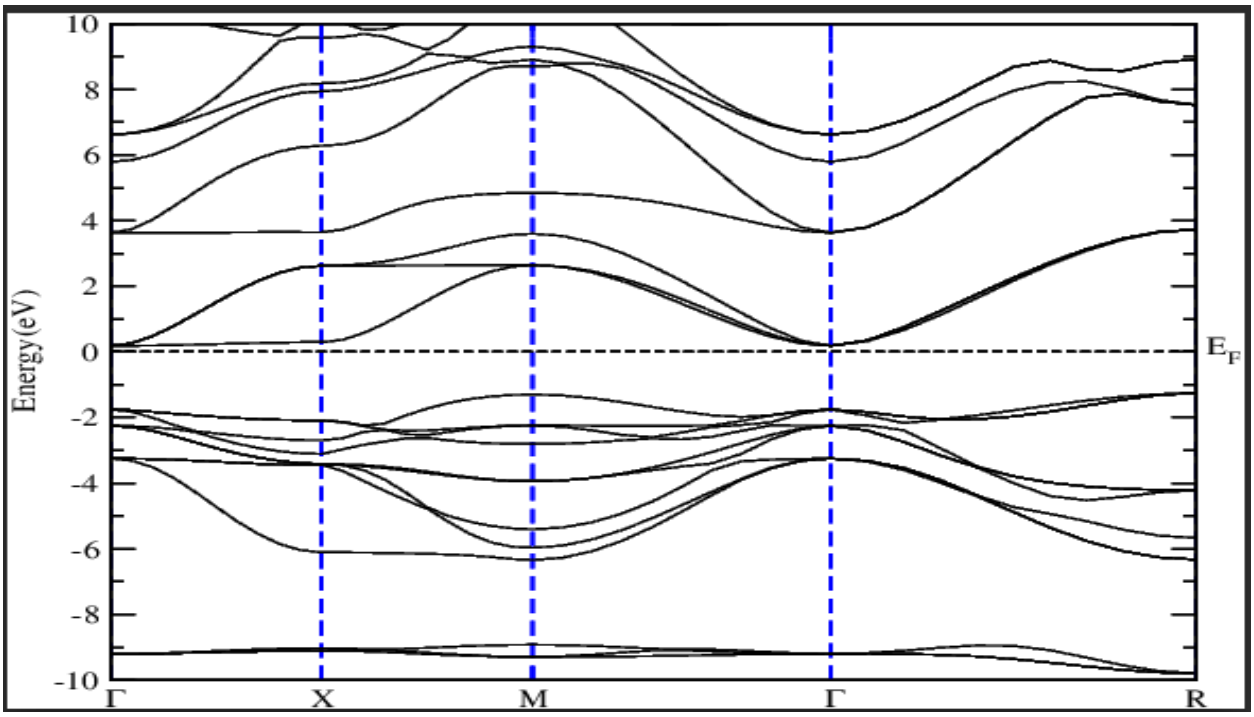

Figure 4.2: Up band spin for $RbNbO_3$ Perovskite compound showing the indirect band gap, confirming it's semiconducting behaviour

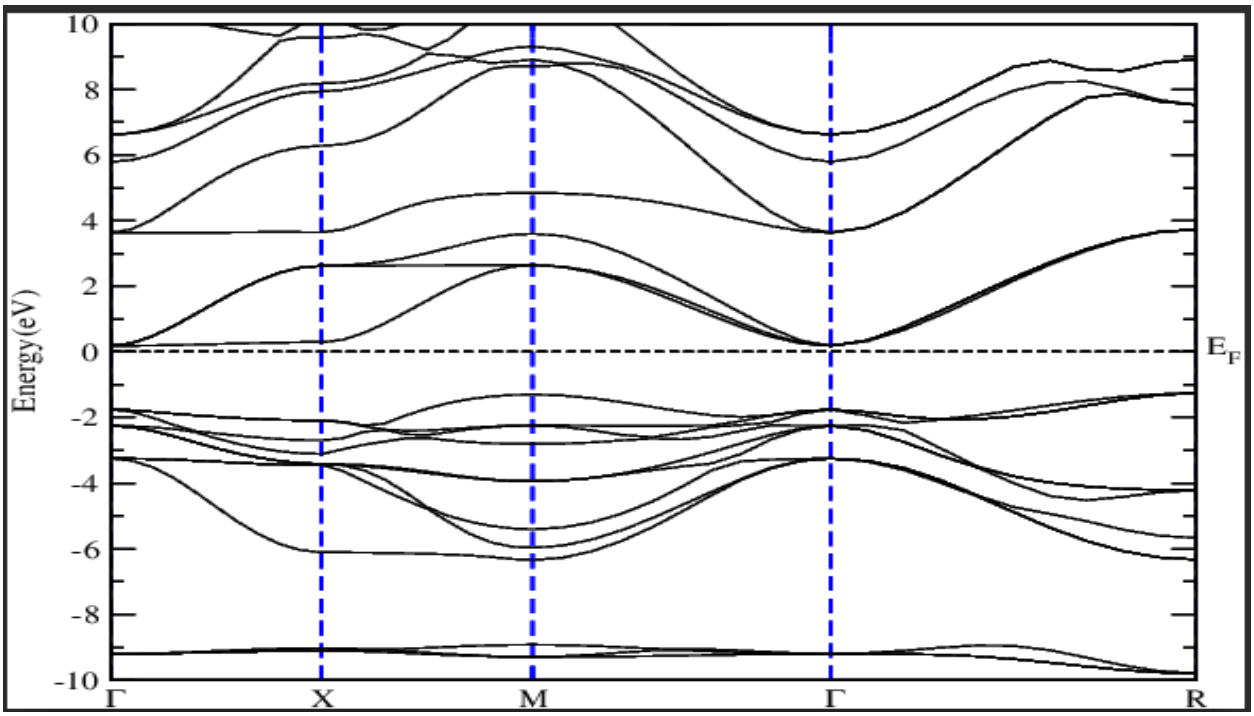

Figure 4.3: Down band spin for $RbNbO_3$ Perovskite compound showing the indirect band gap, confirming it's semiconducting behaviour

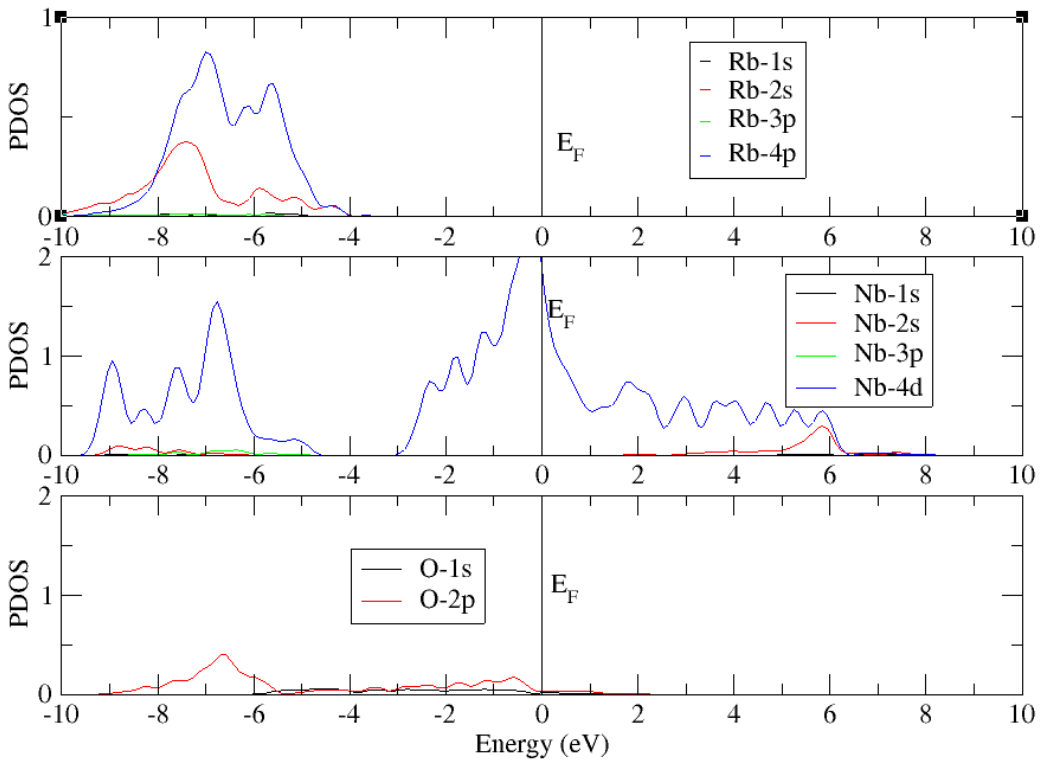

Figure 4.4: Density of state of the $RbNbO_3$ Perovskite compound

From first principle calculations carried out, observations drawn in the case of the electronic properties are as follows;

- $RbNbO_3$ has an indirect band gap, confirming its semiconducting behavior.
- O-2p states dominate the valence band, while Nb-4d states dominate the conduction band.
- Main electronic transitions are O-2p → Nb-4d, showing strong Nb–O bonding.

4.1.4 Phonon and Vibrational Properties

4.1.4.1 Overview of Phonon and Vibrational Properties

The phonon properties describe how atoms vibrate in the crystal lattice and how these vibrations (phonons) interact with each other, electrons, and external stimuli such as temperature or pressure.

In $RbNbO_3$ perovskite (ABO_3):

A = Rb^+ (alkali ion)

B = Nb^{5+} (transition metal)

O = O^{2-} (oxygen anion)

The phonon dispersion and phonon density of state provide insights into structural stability, phase transitions, ferroelectricity, and thermal properties.

4.1.4.2 Phonon Dispersion Relation

The phonon dispersion curve plots phonon frequency (ω) versus wave vector (k).

For dynamically stable structures, all phonon frequencies are positive (no imaginary or negative frequencies).

The presence of imaginary frequencies (negative values) at certain high-symmetry points in the Brillouin zone indicates structural instability or a tendency toward phase transition.

For $RbNbO_3$:

In its cubic phase, phonon dispersion calculations often show imaginary modes at the Γ (Gamma) or R points, signifying ferroelectric instability.

This instability drives a phase transition from the centrosymmetric cubic structure (Pm-3m) to a non-centrosymmetric tetragonal or orthorhombic phase — which is ferroelectric.

Hence, $RbNbO_3$ prefers a distorted perovskite phase, where Nb atoms shift slightly relative to the oxygen octahedra, leading to a spontaneous electric polarization.

4.1.4.3 Vibrational Modes and Their Origin

$RbNbO_3$ has five atoms per primitive cell, yielding 15 vibrational modes (3 acoustic + 12 optical).

Table 4.2: $RbNbO_3$ mode type description grouped based on atomic motion

Mode Type Description	**Dominant Atoms**	**Frequency Range**
Acoustic modes	Low-frequency region	All atoms $< 100\ cm^{-1}$
Low-frequency optical modes	Mainly Rb vibrations against the NbO_6 framework	Rb 50–150 cm^{-1}
Mid-frequency optical modes	Octahedral tilting and Nb–O bending	Nb, O 200–400 cm^{-1}
High-frequency optical modes	Nb–O stretching vibrations	Nb–O bonds 500-800 cm^{-1}

The high-frequency modes are particularly sensitive to Nb–O bond strength and reflect the degree of covalency and distortion in the NbO_6 octahedron.

4.1.4.4 Phonon Density of States (PhDOS)

The PhDOS provides information about how vibrational energy is distributed among the atoms:

Rb contributions dominate the low-energy (acoustic) part of the spectrum, due to its large mass and weak bonding.

Oxygen and niobium dominate the high-energy region, especially in stretching modes.

Negative frequencies in the PhDOS confirm dynamic instability of the relaxed (distorted) phase.

This distribution pattern is typical for perovskites with heavy A-site cations and transition-metal B-sites.

4.1.4.5 Ferroelectric and Lattice-Dynamical Implications

The soft mode (low-frequency polar phonon) at the Γ-point is a key signature of ferroelectric behavior.

As the temperature decreases, this soft mode frequency approaches zero, inducing a spontaneous polarization due to Nb displacement within the oxygen octahedra.

Therefore, $RbNbO_3$ behaves similarly to $KNbO_3$ and $NaNbO_3$, known for their ferroelectric and piezoelectric characteristics.

4.1.4.6 Thermal and Elastic Insights

From phonon spectra, one can also infer:

Debye temperature (ΘD) — relates to lattice stiffness and heat capacity.

Low thermal conductivity — typical in perovskites due to phonon scattering at octahedral tilts.

Anharmonicity — moderate in $RbNbO_3$, contributing to lattice distortions but maintaining overall stability.

From the first principle calculations, phonon and vibrational characteristics of $RbNbO_3$ perovskite includes:

- Dynamic instability in the cubic structure (imaginary modes), leading to spontaneous symmetry breaking.
- Stable vibrational spectra in the distorted (ferroelectric) phase.
- Low frequency modes arise mainly from **Rb vibrations** due to its lighter bonding role.
- Dominant Nb–O stretching modes in the high-frequency region, linked to strong covalent bonding and polarization.

These properties make $RbNbO_3$ a promising ferroelectric and optoelectronic material, suitable for piezoelectric sensors, actuators, and nonlinear optical devices.

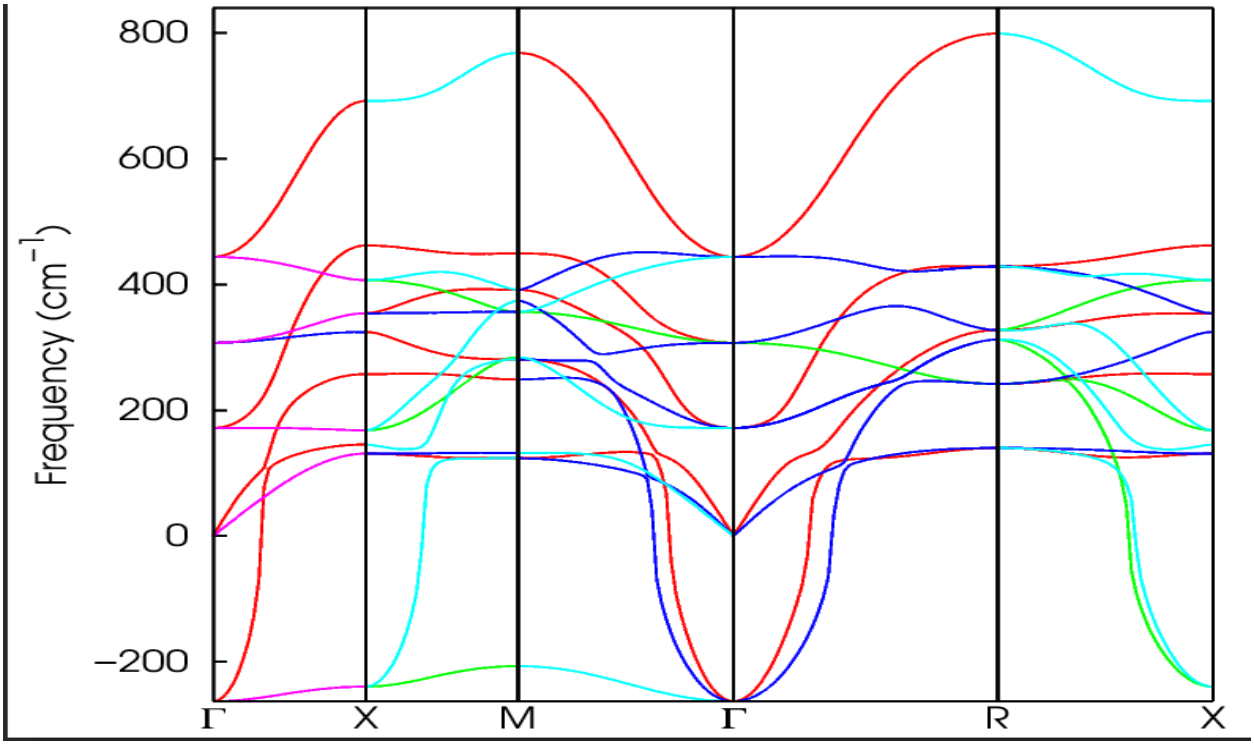

Figure 4.5: Phonon dispersion of $RbNbO_3$ showing lattice vibrations and dynamic instability.

CHAPTER 5

5.1 Findings and Conclusion

The optimization, mechanical properties, electronic band structure, and density of states (DOS) of the perovskite material $RbNbO_3$ were examined through first principle calculations using the quantum espresso program. The computations led to the following findings.

1. The physical properties of $RbNbO_3$ have been studied using density functional theory.
2. From Pugh's ratio (B/G), it shows that the compound is brittle.
3. From the plotted band structure graph, the perovskite compound is a semiconductor.

4. $RbNbO_3$ perovskite is dynamically unstable.
5. $RbNbO_3$ perovskite is mechanically stable.

5.2 Suggestions for Further Studies

The density of states (DOS), electronic band structure, and mechanical characteristics of the perovskite compound $RbNbO_3$ were calculated from first principles. It is recommended that efforts be made to enhance the utilization of $RbNbO_3$ perovskite compound in photochemistry and photovoltaic applications.

REFERENCES

Iyorzor B. E., Babalola M. I. and Ebuwa S.O. Investigating the Effect of Hydrostatic Pressure on the Structural, Electronic, Mechanical, Lattice Dynamics and Optical Properties of the Cubic Perovskite RbTaO3: A DFT Approach (2022)

Zhengqi Shi, Ahalapitiya H. Jayatissa. Perovskites-based solar cells: a review of recent progress, materials and processing methods (2018).

Devendra K. Pandey, Anchit Modi, Padmini Pandey, N.K. Gaur Variable excitation wavelength photoluminescence response and optical absorption in BiFeO3 nanostructures (2017)

Eman Abdul Rahman Assirey, Perovskite synthesis, properties and their related biochemical and industrial application (2019)

J.K. Kim, S.S. Kim, W.-J. Kim. Sol–gel synthesis and properties of multiferroic BiFeO3 (2005)

V. Raghavan. Material Sciences and Engineering (2015)

Robert J. Cava. Oxide superconductors (2008)

K. Singh, A. Maignan, C. Simon, C. Martin .FeCr2O4 and CoCr2O4 spinels: multiferroicity in the collinear magnetic state?(2011)

Peleg Roni. The Perovskite Handbook (2018)
H.M. Christen, G. Eres. Recent advances in pulsed-laser deposition of complex oxides (2008)

Janet Taylor, Ke Zhang, Donghai Wang. Industrial and nonfood applications(2019)

A. Ottochian, G. Dezanneau, C. Gilles, P. Raiteri, C. Knight, J.D. Gale. Influence of isotropic and biaxial strain on proton conduction in Y-doped BaZrO3: a reactive molecular dynamics study (2014)

F. Jia, H. Zhong, W. Zhang, X. Li, G. Wanga, J. Songa, Z. Cheng, J. Yin, L. Gu o. A novel nonenzymatic ECL glucose sensor based on perovskite LaTiO3-Ag0.1 nanomaterials (2015)

Y. Lianghao, C. Yonghong, G. Qingwen, T. Dong, L. Xiaoyong, M. Guangyao, L. Bin. Layered perovskite oxide Y0.8Ca0.2BaCoFeO5+δ as a novel cathode material for intermediate-temperature solid oxide fuel cells (2015)

B. Wang, S. Gu, Y. Ding, Y. Chu, Z. Zhang, X. Ba, Q. Zhang, X. Li. A novel route to prepare LaNiO3 perovskite-type oxide nanofibers by electrospinning for glucose and hydrogen peroxide sensing (2012)

Hongjiao Li, Y. Zhao, Y. Wang, Y. Li. Sr2Fe2−xMoxO6−δ perovskite as an anode in a solid oxide fuel cell: effect of the substitution ratio (2016)

C. Jin, X. Cao, F. Lu, Z. Yang, R. Yang. Electrochemical study of Ba0.5Sr0.5Co0.8Fe0.2O3 perovskite as bifunctional catalyst in alkaline media (2013)